Journal of Nuclear Materials 415 (2011) S849–S851

Contents lists available at ScienceDirect

Journal of Nuclear Materials

journal homepage: www.elsevier.com/locate/jnucmat

Pellet interaction with runaway electrons

A.N. James [a,*], E.M. Hollmann [a], J.H. Yu [a], M.E. Austin [b], N. Commaux [c], T. Evans [d], D.A. Humphreys [d], T.C. Jernigan [c], P.B. Parks [d], S. Putvinski [e], E.J. Strait [d], G.R. Tynan [a], J. Wesley [d]

[a] UC San Diego Center for Energy Research, La Jolla, CA 92093-0417, USA
[b] University of Texas, Austin, TX, USA
[c] Oak Ridge National Laboratory, Oak Ridge, TN, USA
[d] General Atomics, San Diego, CA, USA
[e] ITER Organization, St. Paul-lez-Durance Cedex, France

ARTICLE INFO

Article history:
Available online 26 February 2011

ABSTRACT

We describe results from recent experiments studying interaction of solid polystyrene pellets with a runaway electron current channel generated after cryogenic argon pellet rapid shutdown of DIII-D. Fast camera imaging shows the pellet trajectory and continuum emission from the subsequent explosion, with geometric calibration providing detailed explosion analysis and runaway energy. Electron cyclotron emission also occurs, associated with knock-on electrons broken free from the pellet by RE which then accelerate and runaway, and also with a short lived hot plasma blown off the pellet surface. In addition, we compare heating and explosion times from observations and a model of pellet heating and breakdown by runaway interaction.

1. Introduction

In these experiments, we study runaway electron (RE) generation in tokamak disruptions by inducing a rapid shutdown in otherwise quiescent plasmas through injection of 2.7 mm diameter cryogenic argon pellets [1]. As the pellet streaks through the hot plasma, ablated argon radiates away plasma thermal energy by line emission. RE are first generated during the rapid thermal quench (TQ) which causes a drop in plasma conductivity and an associated loop voltage from the subsequent current quench (CQ). RE then avalanche due small loop voltages compared with those required for initial generation. After the RE avalanche to a current plateau of around half the initial current magnitude, we inject diagnostic pellets to study the interaction with RE current using the various diagnostics available, depicted in Fig. 1.

We observe signatures of the diagnostic pellet impacted by RE on a fast visible imaging camera, an ECE radiometer, and a spectrometer used usually for observing charge exchange recombination, but see no signatures of expected X-ray emission from RE scattering off the pellet (Fig. 2). Fast visible imaging observations suggest the presence of a steep runaway edge gradient. Analysis of cyclotron emission indicates a loop voltage present which exceeds external measurements, indicating the need for a better in-situ measurement and understanding. RE current appears relatively unaffected by the pellets compared to impurity injection experiments at JT-60U [2] and Tore-Supra [3], perhaps due to the smaller amount (10 torr L) and lower atomic number of injected impurities in the present experiments.

2. Impurity pellet injection

For these experiments we used the lithium pellet injector which uses 500 psi = 3.4 MPa helium gas to inject pellets at 700 m/s into RE current plateaus. Up to three 2 × 2 mm pellets can be injected at different times. After testing various materials, we selected polystyrene due to its improved properties for all of the above except a lower vaporization temperature which results in decreased penetration into the RE current. The higher vaporization temperature for carbon makes it a more desirable pellet media, but due to brittleness carbon pellets shatter in the curved guide tube which delivers pellets to the tokamak, and abrasive grinding of carbon against the guide tube walls in a vacuum environment increases variation in pellet delivery velocities.

Monte-Carlo modeling [4] indicates a shower of X-rays emitted from runaways scattering off the solid pellets, however we observed no such emission. This suggests that the RE current density which destroys the pellet is lower than in a simple flattop model, which would result in reduced X-ray emission below our detection threshold.

3. Visible Imaging

As shown in Fig. 3, the Phantom v7.2 visible imaging camera records 12 μs exposures of the pellet traversing the vacuum vessel

* Corresponding and presenting author. Address: UC San Diego Center for Energy Research, 9500 Gilman Dr., La Jolla, CA 92093-0417, USA.
E-mail address: anjames@cer.ucsd.edu (A.N. James).

0022-3115/$ - see front matter © 2011 Elsevier B.V. All rights reserved.
doi:10.1016/j.jnucmat.2011.01.135

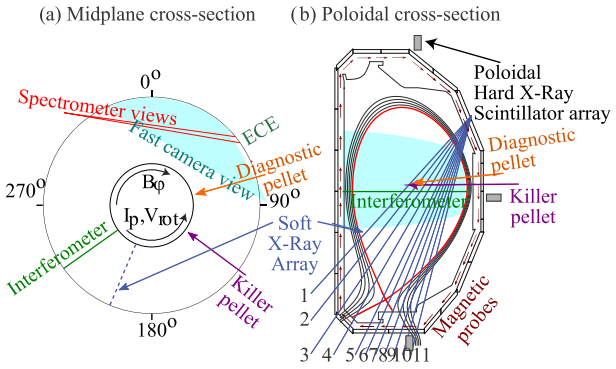

Fig. 1. Layout of diagnostics and experimental hardware used in pellet injection experiments studying RE, with (a) a top down midplane cross-section and (b) a poloidal cross-section. Note that not all diagnostics lie in the same poloidal plane.

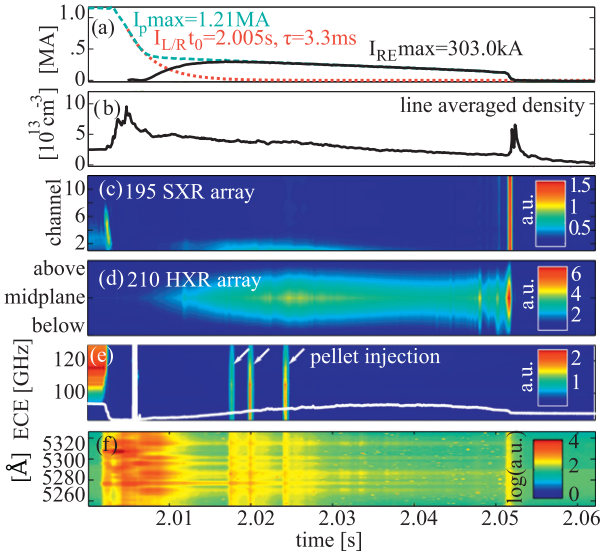

Fig. 2. Traces for the experiment showing (a) plasma current I_p, fit to L/R current decay time, I_{LR}, subtraction of the two for RE current I_{RE}, (b) density, (c) soft X-rays shown by chord number (see Fig. 1), (d) a poloidal array of three hard X-ray scintillators [14], (e) cyclotron emission power spectrum, and (f) a portion of the visible emission spectrum.

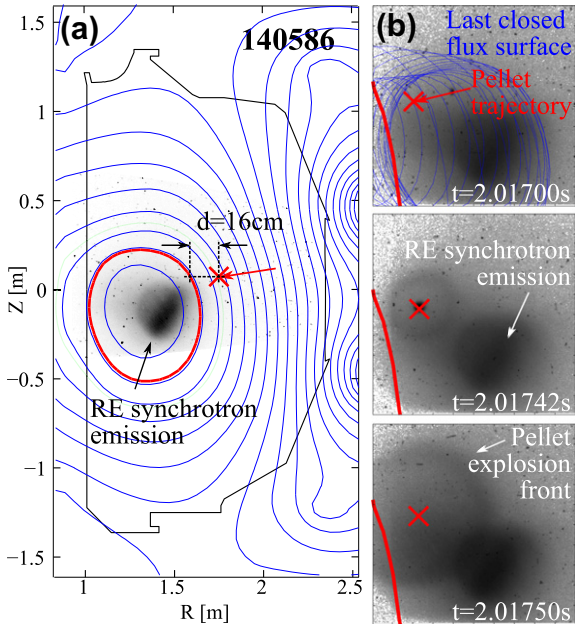

Fig. 3. On the left, (a) a visible camera frame mapped into the poloidal R, Z plane from just before injecting the first pellet. The last closed flux surface, pellet trajectory, and pellet explosion location are marked in red. On the right, (b) a sequence of three images for the first pellet injected, covering the pellet explosion with the background LCFS marked at various toroidal locations in blue, the pellet trajejctory in red, and the LCFS in the plane of pellet injection in red in the foreground. The view spans a curving plasma geometry which we map to the R, Z plane with the tangency points between magnetic field lines and pixel lines of sight, accurate to a few millimeters. (For interpretation of the references to colour in this figure legend, the reader is referred to the web version of this article.)

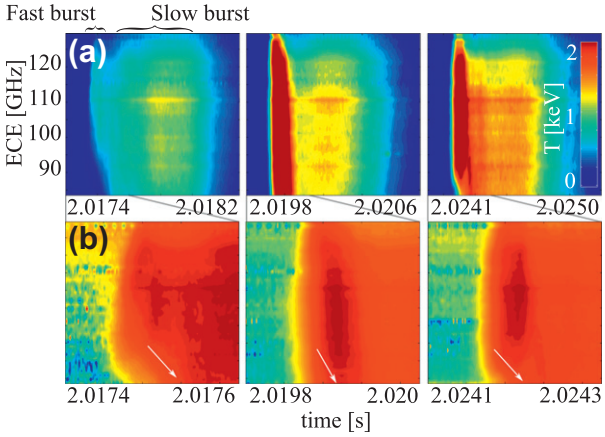

Fig. 4. (a) Cyclotron emission bursts featuring a fast and slow component and (b) a zoom on the fast component in arbitrary log scale, with frequency drift annotated.

illuminated either by cold background plasma or by a low runaway current density until it comes within a few centimeters of the last closed flux surface (LCFS), where it abruptly explodes from RE impact. The camera sees no $\lambda_c \lesssim 700$ nm RE synchrotron emission outside the LCFS, but sees light inside corresponding to $\epsilon_{RE} > (2\rho/3\lambda_c)^{1/3} m_e c^2 = 60$ MeV [5] for radius of curvature ρ, accurate to a factor of 2–3 due to slow cutoff of the synchrotron spectrum and spectral sensitivity of the camera. This indicates the presence of a strong runaway energy and density gradient around the LCFS. Reflectometer measurements in other fast-shutdowns of the cold plasma maintained by RE collisions with background gas reveal a gradient in plasma density supporting this result.

The pellets explode outside of the LCFS, determined by JFIT magnetic reconstructions [6], from interaction with RE confined there due to a relativistic drift orbit displacement effect which also gives us a measurement of RE energy. We measured a pellet velocity of 725 m/s and located the pellet explosions to roughly $d = 16$ cm outside of the last closed flux surface (see Fig. 3a annotation). Passive spectroscopy of ion emission in the cold background plasma indicates a temperature of roughly 1.5 eV and single ionization, too cold to cause a pellet explosion. From the observed displacement and a JFIT calculation of $q_a = 6$, we calculate a rough measure of RE energy [7] of $W_R = \text{decB}/q = 17$ MeV for RE which destroy the pellet. We also note that this apparent displacement may also be caused by diffusive transport of runaways outside of the LCFS. Visible synchrotron emission in the core suggests high energy RE there, and lower energy RE synchrotron emitting invisible infrared outside the LCFS which destroy the pellet. Continuum emission (Fig. 2f) from the explosion front (Fig. 3b) expands at a velocity of $v = 1200$ m/s, corresponding to a temperature of 750 K for a CH, $m = 13$ amu gas.

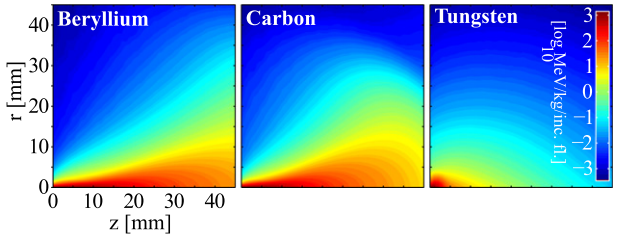

Fig. 5. Energy deposition simulation using EGSnrc for a pencil beam of 20 MeV RE impacting various materials from the left at $r = 0$, $z = 0$.

4. Cyclotron emission

Just after the pellet explosion, we see a burst of ECE with a fast ~10 μs component and a slow ~100 μs component, shown in Fig. 4 for each of the three injected pellets. The fast component intensity varies per pellet in equivalent plasma temperature from below 1 keV to above 5 keV and may represent emission from non-thermal knock-on electrons from the pellet with the emitted spectrum determined by the knock-on energy spectrum described previously [8]. The slow component seems to remain more constant pellet to pellet at around 1 keV between the three pellets and may correspond to hot plasma blown off of the pellet or thermal electrons heated by collisions with low energy non-thermals. The fast emission frequency drops at a rate of $d\omega_c/dt = -183$ GHz/ms which suggests a relativistic increase in mass as knock-on electrons from the pellet accelerate. The corresponding rate of acceleration would be

$$d\epsilon/dt = -\gamma^2 m_e c^2 (m_e/eB) d\omega_c/dt = 1\ \mathrm{MeV/ms} \quad (1)$$

which corresponds to an effective local loop voltage of at least 35 V assuming zero drag and electrons moving at the speed of light. Non-thermal electrons at subluminal velocities would experience a greater drag and hence would correspond to an even greater voltage, but without an accurate measure of these electrons' starting energy we cannot estimate that voltage. In either case however, this loop voltage significantly exceeds the zero dimensional loop voltage measured by external coils at this time.

5. Pellet heating and breakdown by RE

We consider RE energy of $E_{RE} = 17$ MeV corresponding to the observed displacement, and a flattop RE current profile spread uniformly throughout the cross-sectional area $A_{RE} = .36\ \mathrm{m}^2$ of $j_{RE} = 512\ \mathrm{kA/m}^2$. At this energy the stopping power in polystyrene $s \sim 2.5\ \mathrm{MeV\,cm}^2/\mathrm{g}$ [9] corresponds to a mean free path of about 7 cm which exceeds the pellet size, resulting in volumetric heating instead of a slower ablation type pellet burn observed and thoroughly modeled for pellets injected into hot plasmas [10–12]. The volumetric heating power

$$Q = (j_{RE}/e)(dE/dx) = \rho s j_{RE}/e \sim 125\ \mathrm{MW/cm}^3 \quad (2)$$

results in a temperature rise rate of $dT/dt = Q/C\rho = 100$ K/μs at this power density which takes only a few microseconds to melt and vaporize the pellet.

This simple model does not describe the energy deposition within larger pellets or different materials, which we studied with a Monte-Carlo transport model [4] of various energy electrons impacted onto slabs of beryllium, carbon, and tungsten as shown in Fig. 5. This reveals a shallower and narrower penetration for higher atomic number (Z) materials, indicating a more lathe-like ablation of these pellets. Conversely, RE may penetrate multiple centimeters of low-Z materials; hence even large pellets may explode.

The pellet temperature continues to grow after melting until power loss from evaporation at the surface and thermal radiation balance runaway heating and clamp the temperature, as described in detail elsewhere [13]. Where core temperature exceeds the vacuum boiling point, the liquid will break up by vapor bubbles into smaller and smaller fragments until surface tension balances evaporation at the smallest sizes, when droplet core temperature may increase again. Since runaway energy exceeds the enthalpy for evaporation $E_{ev} \sim .73$ eV/molecule by orders of magnitude, it is also possible for direct sublimation to occur before bulk heating causes melting and evaporation. Camera observations have neither the spatial or temporal resolution to discriminate between these processes.

6. Conclusions

We observed explosion of injected pellets upon contact with RE, suggesting a volumetric heating by penetrating RE. The cyclotron emission burst frequency drift observed indicates a local loop voltage of greater magnitude than externally measured, suggesting the need for improved in-situ loop voltage measurements and understanding. Comparison of the pellet heating and explosion rate agrees with modeling and a theory for pellet breakdown by RE impact within an order of magnitude. These observations combined contribute improvements to our understanding of RE confinement, acceleration, and interaction with materials.

Acknowledgments

The authors would like to acknowledge Gary Jackson, Jim Kulchar, Derek Sundstrom, Ron Ellis, David Ayala, and Matthew Watkins at DIII-D for assistance with re-installation of the lithium pellet injector system which enabled these experiments.

This work supported by the US Department of Energy under DE-FG02-07ER54917, DE-FG02-07ER54912, DE-FG03-97ER54415, DE-AC05-00OR22725, and DE-FC02-04ER54698.

References

[1] T. Evans, in: Proceedings of the 17th International Atomic Energy Agency Fusion Energy Conference, 1999.
[2] Y. Kawano, T. Nakano, A. Isayama, N. Asakura, H. Tamai, H. Kubo, H. Takenaga, M. Bakhtiari, S. Ide, T. Kondoh, T. Hatae, J. Plasma Fusion Res. 81 (2005) 593–601.
[3] F. Saint-Laurent, in: Proceedings of the 36th European Physical Society Conference, 2009.
[4] I. Kawrakow, NRCC Report PIRS-701 (2009).
[5] J. Jackson, Classical Electrodynamics, third ed., John Wiley and Sons, Inc., Hoboken, New Jersey, 1998, p. 679.
[6] D.A. Humphreys, A.G. Kellman, Phys. Plas. 6 (1999) 2742–2756.
[7] I. Entrop, Confinement of Relativistic Runaway Electrons in Tokamak Plasmas, Ph.D. thesis, Technische Universiteit Eindhoven, 1999.
[8] R. Jayakumar, H.H. Fleischmann, S.J. Zweben, Phys. Lett. A 172 (1993) 447–451.
[9] M.J. Berger, J.S. Coursey, M.A. Zucker, J. Chang, NISTIR 4999 (1993).
[10] P.B. Parks, R.J. Turnbull, Phys. Fluids 21 (1978) 1735–1741.
[11] L. Baylor, A. Geraud, W. Houlberg, D. Frigione, M. Gadeberg, T. Jernigan, J.D. Kloe, P. Kupschus, B. Kuteev, P. Lang, A. Oomens, A. Qualls, K. Sato, G. Schmidt, Nucl. Fusion 37 (1997) 445.
[12] V.Y. Sergeev, O.A. Bahaeva, B.V. Kuteev, M. Tendler, Plas. Phys. Rep. 32 (2006) 363–377.
[13] S. Putvinski, ITER Internal Report – ITER-D-2MJPGH, 2009.
[14] A.N. James, E.M. Hollmann, G.R. Tynan, Rev. Sci. Instrum. 81 (2010) 10E306, doi:10.1063/1.3475710.